Generation of 0.4-keV Femtosecond Electron Pulses using Impulsively Excited Surface Plasmons

S. E. Irvine,* A. Dechant, and A. Y. Elezzabi

Ultrafast Photonics and Nano-Optics Laboratory, Department of Electrical and Computer Engineering, University of Alberta, Edmonton, Alberta, Canada T6G 2V4

(Received 25 March 2004; published 28 October 2004)

We demonstrate the generation of 0.4-keV, sub-27 fs electron pulses using low-intensity laser pulses from a Ti:sapphire oscillator through the excitation of surface plasmon waves on a time scale within the plasmon lifetime. Modeling of the ponderomotive electron pulse acceleration yields electron energy spectra that are in excellent agreement with the observed ones. Our work opens a doorway for time-resolved experimentation using low-power, high-repetition rate laser pulses.

DOI: 10.1103/PhysRevLett.93.184801 PACS numbers: 41.75.Jv, 73.20.Mf, 79.60.–i

Ultrafast electron pulses are used to reveal the hidden dynamics of intricate molecular and atomic processes through experimentation such as time-resolved electron diffraction [1] and femtochemistry [2]. Of particular interest are investigations of ultrafast coherent events occurring on time scales of ~5–25 fs, which require ultrafast electron pulses with comparable durations. The most intriguing ultrafast electron pulse sources are those employing femtosecond lasers. While high-power lasers can produce ultrashort pulses with large electric fields, $E_l(t)$, the transverse nature of electromagnetic radiation does not allow for direct acceleration of charged particles, and complex designs, such as postphotoemission acceleration grids [3] or wakefield accelerators [4], must be implemented. However, significant electron acceleration can be achieved by exploiting the ponderomotive potential of a high spatial gradient electromagnetic field. Furthermore, by localizing the electromagnetic field to a region of space smaller than the wavelength ($< \lambda_l$), an enhancement of the electric field density, and hence ponderomotive force, can be achieved. When $E_l(t)$ is used to excite surface plasmon (SP) waves in a thin metallic film, the electromagnetic field is confined near the metal surface in the form of a surface wave. Not only does the collective oscillation of the SP field, $E_{\mathrm{SP}}(z, t) \sim \eta E_l(t) \times \exp(-\alpha z)$, enhance $E_l(t)$ by a factor of η ($\sim 10^2$–10^3), but also it creates a high spatial gradient as the field exponentially decays within a characteristic length α^{-1} ($< \lambda_l$). Introducing electrons into $E_{\mathrm{SP}}(z, t)$ results in large accelerations, as these electrons experience unequal forces during the subsequent oscillations of the SP wave. However, effective energy gain requires precise spatial overlap and a high degree of synchronization between $E_{\mathrm{SP}}(z, t)$ and the electrons. Injecting electrons with the correct phase can be achieved by invoking the multiphoton emission process of the same metal film used to launch the SP's. Here, electrons are simultaneously photoexcited and accelerated by the incident laser pulse, preserving the necessary phase relationship and spatial overlap between the generation and the acceleration mechanisms. This process provides all-optical generation and acceleration that is well suited for time-resolved experiments requiring optical pumping and electron beam probing.

Using the Kretschmann configuration for SP coupling and amplified ~150 fs pulses, Zawadzka *et al.* [5,6] demonstrated the potential for SP-assisted electron acceleration. At an intensity of $I_l = 40$ TW/cm^2 ($E_l = 3 \times 10^8$ V/cm), 0.4 keV electrons were produced. Similar experiments by Kupersztych *et al.* [7] also demonstrated SP-assisted electron acceleration using a metallic grating structure. Here, 60 fs pulses at an intensity of $I_l = 8$ GW/cm^2 ($E_l = 2.5 \times 10^6$ V/cm) were employed to produce electrons with energies up to 25 eV. By further increasing the pulse duration to 800 fs, with intensity of $I_l = 3.2$ GW/cm^2 ($E_l = 1.5 \times 10^6$ V/cm), 40 eV electrons were produced. Notably, the SP waves in these experiments were excited using laser pulses having durations longer than the lifetime of the SP waves ($\tau_{\mathrm{SP}} \sim 48$ fs) [8], and the peak amplitude of the plasmon wave had diminished before efficient electron acceleration could be achieved. To take full advantage of the enhanced $E_l(t)$, the SP waves should be excited on time scales shorter than τ_{SP}.

In this Letter, we present experimental evidence for high-energy electron acceleration using impulsively excited SP's. High-energy electrons, up to 0.4 keV at a repetition rate of 80 MHz, are generated. To our knowledge, this is the first observation of high-energy electron acceleration using unamplified (~ 1.5 nJ) pulses delivered by a Ti:sapphire oscillator. This opens a doorway for the generation of electron pulses using low-power laser systems, and is a fundamental step toward the development of reliable, compact, ultrashort, high-repetition rate systems for sensitive time-resolved electron pulse experiments. To further the understanding of the experimental data, an ultrafast photoemission and acceleration simulation (UPAS), based on multiphoton absorption and the

finite-difference time-domain (FDTD) technique, is implemented.

SP waves are excited using transverse magnetic polarized 27 fs, 800 nm laser pulses from a Ti:sapphire oscillator, delivering 1.5 nJ pulses at 80 MHz. To couple the laser pulses into SP oscillations, we employ the Kretschmann geometry where a 50 nm Ag film has been deposited on a silica prism. The laser pulses are focused onto the Ag film to a spot size of 60 μm, and the angle of incidence is adjusted to maximize the electron emission. The prism assembly is placed inside a vacuum chamber which is evacuated to a pressure of $\sim 10^{-5}$ Torr, and the photocurrent is monitored using a single channel electron multiplier (Ceremax 7596, zero postacceleration) having a collection angle of 0.28 sr. The kinetic energy distribution of the electron pulse is measured using the retarding potential method.

The nature of the emission process determines the shape of the kinetic energy spectra of the electron pulses. In the presence of a high-intensity laser field, two ionization regimes exist for metal surfaces: multiphoton ionization ($\gamma \gg 1$) and tunnel ionization ($\gamma \ll 1$) [9]. Here, $\gamma = \omega(2mW_f)^{1/2}/eE_l$ is the Keldysh parameter, where ω is the frequency of the laser field, m and e are the mass and charge of the electron, and W_f is the work function of the metal. Using our experimental parameters, $W_f = 4.26$ eV (for Ag) and $E_l = 1.2 \times 10^6$ V/cm, γ equals 26, which is indicative of a multiphoton process. To ascertain the electron photoemission mechanism, the dependence of the photocurrent (i_{ph}) on incident intensity is measured. Figure 1(a) displays the results of such an experiment demonstrating a third-order intensity dependence ($\propto I_l^3$), showing clear evidence that the electron emission is a three-photon photoemission (3PP) process. On the contrary, with the excitation of SP waves it is expected that the electric field at the metal surface will be enhanced by η, thus reducing γ to ≤ 0.26, and indicating that the emission process should be dominated by tunnel ionization. While the presence of the SP waves enhances the coupling of E_l into the film, the dominance of multiphoton ionization supports the fact that E_{SP} does not independently contribute to the electron emission process. Since electron emission occurs only during the presence of E_l, as evidenced by the 3PP characteristic of Fig. 1(a), the electron pulse duration can be inferred directly from a 3PP-correlation $i_{\mathrm{ph}}(\tau) = \int_{-\infty}^{\infty}([E_l(t-\tau) + E_l(t)]^2)^3 dt$. Figure 1(b) displays an interferometric two-pulse 3PP-correlation trace for a 27 fs incident laser pulse, indicating that at the surface of the film, the electron pulse duration is ≤ 27 fs.

Shown in the inset of Fig. 1(a) are the various channels associated with multiphoton bound-free electron transitions, illustrating both coherent and incoherent processes. For the incoherent 3PP channels, finite lifetime intermediate states ($|2\rangle$ and $|3\rangle$) exist between the subsequent absorption of photons. These intermediate states are accessible only through momentum conservation, which can be satisfied through phonon, impurity, or surface scattering [10], resulting in dephasing of the photoexcited electrons with respect to the exciting laser field. In the coherent 3PP channel ($|1\rangle$ to $|4\rangle$), however, electrons are born in phase with both the optical field and the SP field, as there is no change in their respective momenta. As well, the plasmon dephasing time ($\tau_{\mathrm{SP}} \sim 48$ fs) is longer than the optical field pulse duration ($\tau_l = 27$ fs), and thus the excited plasmons remain coherent throughout the entire generation and acceleration intervals. Since electrons are generated only over the duration of the optical pulse (near the peak intensity, $i_{\mathrm{ph}} \propto I_l^3$), they experience the maximum ponderomotive force, and escape the ponderomotive potential before the dephasing of the SP. As a result, the kinetic energy spectrum of the accelerated electrons is shifted toward higher energies, and since most of the electrons have similar energies, one would expect a narrow spectrum. Figure 2 shows a typical kinetic energy spectrum of the electron pulses. At the highest power density, the charge per pulse is measured to be 15 aC. The most striking features of this distribution are its large central value of 0.315 keV and its 83 eV full width at half maximum (only 26% of the center value). Despite the fact that the intensity in our experiments ($I_l = 1.8$ GW/cm^2) is 4 orders of magnitude lower than the previously reported values ($I_l = 40$ TW/cm^2) produced from 150 fs pulses [5], similar maximum kinetic

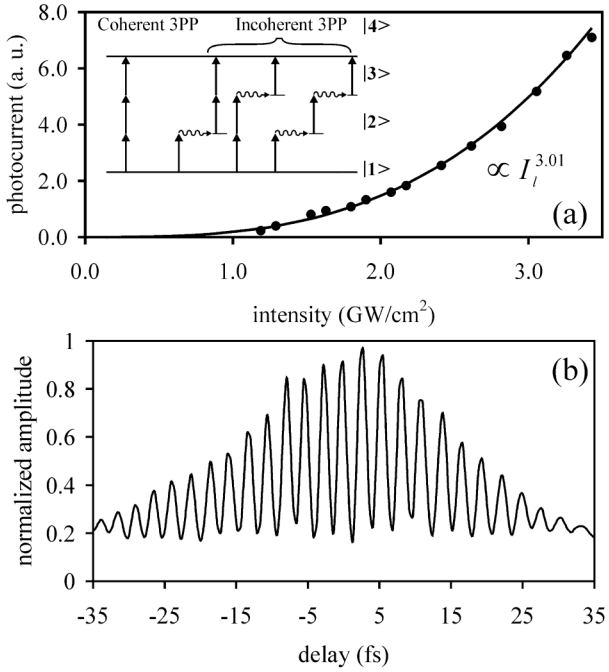

FIG. 1. (a) Measured photocurrent dependence vs intensity, verifying a three-photon process. The inset illustrates the various channels of electron emission, both coherent and incoherent. (b) Measured interferometric two-pulse 3PP-correlation trace for 27 fs laser pulses, indicating that at the surface of the film, the electron pulse duration is ≤ 27 fs.

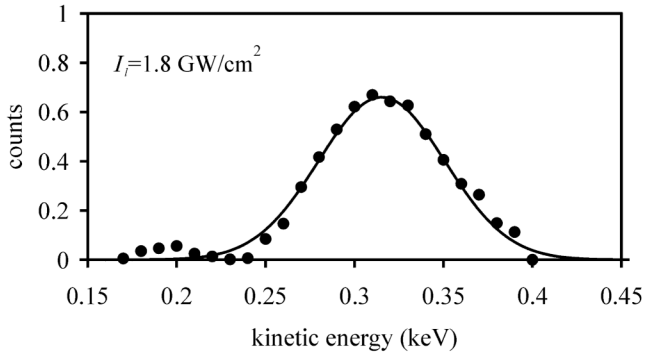

FIG. 2. Experimental kinetic energy distribution of the femtosecond electron pulses.

energies and much narrower spectra are obtained. Previous low-intensity ($I_l = 0.7$ GW/cm^2 produced from 150 fs pulses) experiments in Au by the same group [6] reported electron energies of only ~20 eV with a maximum of 40 eV at $I_l = 21$ GW/cm^2. In these long pulse duration experiments, an increase of intensity by 10^3 increased the maximum electron energies by only a factor of 10 while maintaining the overall broad shape of the energy spectrum. Indeed, our results clearly indicate that efficient electron acceleration requires subplasmon lifetime excitation pulses ($\tau_l < \tau_{SP}$).

To explore the electron generation and acceleration theoretically, we have implemented the UPAS model [11]. This model is composed of two components: (1) FDTD calculation of the electromagnetic field and (2) placement of electrons in the electromagnetic field. For the first portion of the model, SP coupling to the metal film is accounted for through the Drude model [12] for the dielectric function $\varepsilon(\omega) = \varepsilon_0\varepsilon_\infty + \varepsilon_0\omega_p^2(i\omega\nu_d - \omega^2)^{-1}$, where ω_p is the plasma frequency, ν_d is the damping frequency, ε_∞ is the dc dielectric constant, and ε_0 is the permittivity of free space. Following the formalism presented in [13], $\varepsilon(\omega)$ is incorporated into an FDTD method using the auxiliary differential equation method, in which a supplementary equation for the displacement, $\vec{D}$, and electric field, $\vec{E}$, vectors is obtained:

$$\nu\frac{d\vec{D}}{dt} + \frac{d^2\vec{D}}{dt^2} = \omega_p^2\varepsilon_0\vec{E} + \nu\varepsilon_\infty\varepsilon_0\frac{d\vec{E}}{dt} + \varepsilon_\infty\varepsilon_0\frac{d^2\vec{E}}{dt^2}. \quad (1)$$

This equation, along with Maxwell's curl equations for $\vec{D}$ and $\vec{H}$ are solved using a central differencing technique [13]. Once the electromagnetic field distribution of the SP is determined from the FDTD algorithm, it can be used in the second stage of the UPAS model, in which the trajectories of a large number of electrons are calculated. Spatially, the electrons are placed around the peak of the pulse (within ~10% of the full width at half maximum). Temporally, electrons are distributed around the center of the pulse, and each is weighted according to the intensity at the instant of the electron's emission. Since the process is a third-order multiphoton emission process, the weight is proportional to $I_l^3(t)$. Once the electrons are placed in the electromagnetic field, the Lorentz force equation, $\frac{d\vec{v}}{dt} = qm^{-1}(\vec{E} + \mu_0\vec{v}\times\vec{H})$, is used to determine the velocity and position of the photoelectrons. Electron trajectories, ignoring electron-electron interactions, are mapped to determine the final energies at the detector position.

Figure 3(a) illustrates a snapshot of the spatial distribution of the electric field during the excitation of the SP wave at the dielectric-metal-vacuum interface, as calculated by the FDTD simulation. The electric field associated with the plasmon decays exponentially away from the metal surface with $\alpha^{-1} = 240$ nm, and a high-gradient electric field, $|\nabla_\perp\vec{E}_{SP}| = 8\times10^{13}$ V/cm^2, is observed at the surface of the film. Typical electron trajectories are also calculated from the model. Figure 3(b) illustrates the complex motion experienced by electrons in the presence of intense oscillating electric and magnetic fields. The "quivering" trajectory of a solitary 0.3 keV electron is demonstrated in Fig. 3(c). The "quiver length," defined to be the distance between inflection points of the electron trajectory, is calculated to be ~23 nm. It is also shown in Fig. 3(c) that in 20 fs this electron has traversed a distance of 200 nm. Figure 3(d) displays the evolution of the velocity components, ν_x and ν_y, in time and indicates that within 20 fs, the 0.3 keV

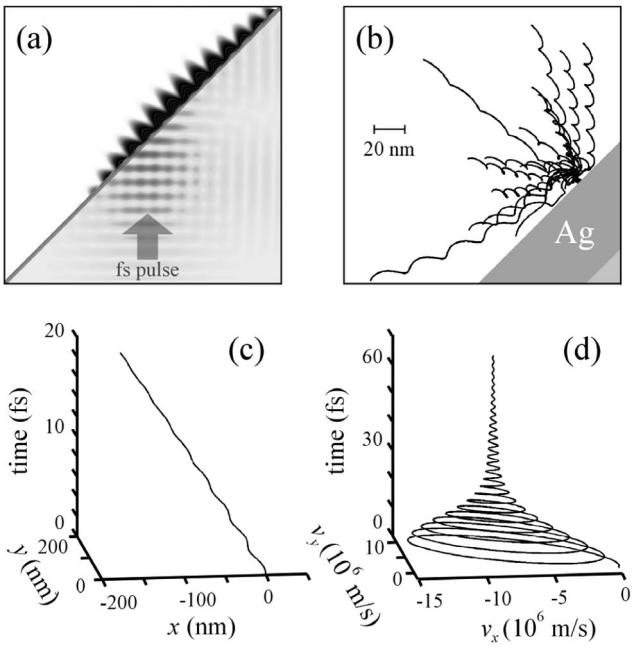

FIG. 3. (a) Calculated electromagnetic field distribution for coupling between a 27 fs pulse and SP waves in a 50 nm Ag film. (b) Electron trajectories, as calculated by the UPAS code, demonstrate the quivering motion of electrons placed in the SP enhanced electromagnetic pulse. (c) Calculated trajectory and (d) velocity components of a solitary 0.3 keV electron, which illustrate the net gain of energy of the electron in the presence of the ponderomotive potential of the SP.

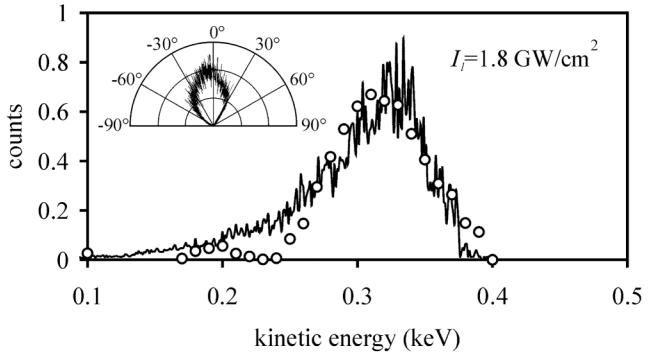

FIG. 4. Experimental (circles) and calculated (solid line) kinetic energy distributions of the SP-assisted femtosecond electron pulse generation. The inset shows the angular (in-plane) distribution of the electron pulses as calculated by UPAS.

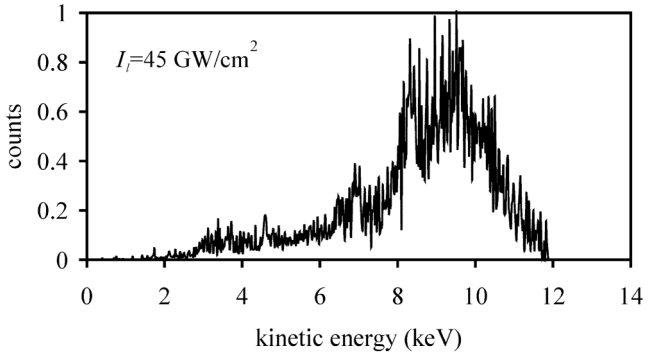

FIG. 5. Calculated kinetic energy distribution of SP-assisted femtosecond electron pulse generation. In this case, the peak SP electric field is a factor of 5 times higher than that used to simulate the data of Fig. 4.

electron has gained virtually all ($> 90\%$) of its net kinetic energy from the ponderomotive field, yielding an effective acceleration gradient of 1.5 GeV/m. In order to calculate the energy distribution of the accelerated electrons, 2.5×10^5 electrons were launched into the SP field with $E_{SP} = 1.8 \times 10^9$ V/cm. It should be noted that 32% of the test electron trajectories return to the Ag film, but do not acquire a significant amount of energy from the ponderomotive field for secondary electron emission, and thus are neglected in calculating the energy spectrum. The SP enhancement for a pulse train of 27 fs is calculated to be 1 order of magnitude for a perfectly smooth (ideal) metal film. However, surface roughness effects (< 50 nm) alter the spatial distribution of the SP field [5,6,14], and are not included in the UPAS code. In such cases, the overall energy of the pulse is conserved, but the energy density is drastically increased by confinement of the pulse to a small volume. As a result, the increase in energy density appears as a localized electric field enhancement, even though the total energy is constant. A full account of surface roughness requires full 3D-FDTD calculation [14], which over the length scales of electron emission and acceleration, requires enormous computational effort in comparison to the current model and is not feasible at this time. A solution is realized by considering an overall effective η. This factor was determined by comparing the model results with those of the experiment, as shown in Fig. 4. Since the two are in excellent agreement, the effective enhancement factor of $\sim 10^3$ is determined. The calculated angular distribution of the ponderomotively accelerated electrons is shown in the inset of Fig. 4, and agrees well with the data presented in [5,6]. Furthermore, the potential of SP-assisted ponderomotive acceleration can be deduced from the model. As shown in Fig. 5, by increasing I_l to 45 GW/cm^2, electrons with energies up to 12 keV can be generated. This agrees well with the linear scaling relationship between the ponderomotive potential and I_l.

The presented work demonstrates the generation of high-energy ultrashort electron pulses using low-intensity optical pulses, opening the doorway for novel time-resolved investigations. We have shown that when the SP is impulsively excited, 0.4-keV sub-27 fs electron pulses are generated. By using higher intensity laser pulses with durations at or below 27 fs, it is predicted, using UPAS, that electrons with keV energies can be generated.

This work is supported by the National Sciences and Engineering Research Council of Canada (NSERC). S. E. I. gratefully acknowledges NSERC.

*Electronic address: irvine@ece.ualberta.ca

[1] B. J. Siwick *et al.*, Science **302**, 1382 (2003).
[2] A. H. Zewail, Science **242**, 1645 (1988).
[3] M. Y. Schelev *et al.*, Opt. Eng. **37**, 2249 (1998).
[4] T. Tajima and J. M. Dawson, Phys. Rev. Lett. **43**, 267 (1979).
[5] J. Zawadzka *et al.*, Appl. Phys. Lett. **79**, 2130 (2001).
[6] J. Zawadzka *et al.*, Nucl. Instrum. Methods Phys. Res., Sect. A **445**, 324 (2000).
[7] J. Kupersztych, P. Monchicourt, and M. Raynaud, Phys. Rev. Lett. **86**, 5180 (2001).
[8] M. van Exter and A. Lagendijk, Phys. Rev. Lett. **60**, 49 (1988).
[9] C. Toth, G. Farkas, and K. L. Vodopyanov, Appl. Phys. B **53**, 221 (1991).
[10] H. Petek and S. Ogawa, Prog. Surf. Sci. **56**, 239 (1997).
[11] S. E. Irvine and A. Y. Elezzabi (to be published).
[12] N. Peyghambarian, S. W. Koch, and A. Mysyrowicz, *Introduction to Semiconductor Optics* (Prentice-Hall, Englewood Cliffs, NJ, 1993).
[13] A. Taflove, *Computational Electrodynamics* (Artech House, Boston, 1995).
[14] The additional SP field enhancement of ~ 40 was calculated for a single ~ 15 nm Ag particle on a metal surface using 3D-FDTD.